RSC Advances

PAPER

View Article Online
View Journal | View Issue



Cite this: *RSC Adv.*, 2025, **15**, 25337

# Engineered single chain variable fragments (scFvs) with improved pH-dependent kinetics for use in continuous biosensor applications†

Ellie D. Wilson, [a] David Probst, [a] Mai Hamasaki,[ab] Miho Oda, [ab] Varun Kochar, [a] Qianming Xu, [b] Ayumi Tanaka,[b] Hirobumi Suzuki, [b] Ryutaro Asano [b] and Koji Sode *[a]

One challenge in the continuous monitoring of insulin lies with the unavailability of a high-affinity biological recognition element (BRE) with kinetic parameters sufficient to track fluctuating concentrations of insulin *in vivo*. An approach to overcome this limitation is to engineer a high-affinity BRE to selectively modulate its binding kinetics in response to an external signal. Herein, we design and evaluate changes in the pH-dependent binding kinetics of an anti-insulin single chain variable fragment (scFv) we previously employed in a point-of-care insulin sensor. We predicted the scFv structure in complex with human insulin and selected scFv residues directly involved in insulin binding for histidine substitution. We identify one mutation, T32H, that improves the pH-sensitivity of the wild-type (WT); the $K_D$ of the T32H mutant is calculated to be 145.5 ± 83.1 nM at pH 7.4 and 17.4 ± 5.1 nM at pH 6.0 – an average of an 8.4× difference between the two conditions and a 3.8× increase in pH-sensitivity from the WT. We design a bio-layer interferometry (BLI) assay to interrogate the improved pH-sensitivity of the T32H mutant in tracking fluctuating insulin concentrations in dynamic pH conditions and find that improved pH-sensitivity can be leveraged to improve biosensor regeneration. These results suggest the potential for pH-sensitive antibodies to improve the development of *in vivo* continuous monitoring systems.

Received 23rd March 2025
Accepted 30th June 2025

DOI: 10.1039/d5ra02051d

rsc.li/rsc-advances



## Introduction

Insulin is a peptide hormone essential in maintaining glucose homeostasis.[1] Patients with diabetes of varying pathophysiology experience hyperglycemia resulting from ineffective insulin production, impaired insulin action, or both.[2] Insulin administration therefore remains a frontline therapy for patients. Exogenous insulin therapy, especially for individuals with type 1 diabetes, has been shown to better regulate glycemic levels and improve overall disease management.[3] Continuous glucose monitors (CGMs) are often used alongside automated insulin delivery (ADI) systems to maintain normoglycemia.[4,5] However, insulin administration within ADI systems is driven solely by glucose-correlated algorithms rather than combined inputs with real-time insulin measurements,[6] and hypoglycemia due to the over administration of insulin remains a risk for patients. Recent research has thus focused on developing biosensors to monitor insulin. Current reported biosensors for insulin monitoring employ either antibodies, aptamers, or insulin receptors as a biological recognition element (BRE).[7] However, these developments have largely been single-use disposable-type sensors that can be utilized for point-of-care testing. The development of a continuous insulin biosensor to reduce the incidence of hypoglycemia and enable tighter glycemic regulation has yet to be realized.

The CGMs on the market today are an ideal example of how the *in vivo* continuous monitoring of biomarkers using biosensors can inform therapeutic interventions and improve clinical outcomes.[8–11] However, the commercialization of biosensors suitable for continuous monitoring of insulin and other protein/peptide biomarkers of interest remains understandably stagnant, as the challenges involved in its realization are both complex and multivariate.[12] Biosensors for *in vivo* continuous monitoring have many requirements, including the use of a sensitive, specific, and reversible BRE. The required sensitivity and specificity of BREs depend on the *in vivo* concentrations of target molecules and how quickly these concentrations fluctuate, while regeneration of the molecular recognition site is crucial to transduce multiple measurements. One challenge in monitoring insulin continuously lies within the tradeoff of specificity and capacity for repeated measurements when using high-affinity BREs.[13]

[a]*Lampe Joint Department of Biomedical Engineering, The University of North Carolina at Chapel Hill, North Carolina State University, Chapel Hill, NC, 27599, USA. E-mail: ksode@email.unc.edu*

[b]*Department of Biotechnology and Life Science, Graduate School of Engineering, Tokyo University of Agriculture and Technology, 2-24-16 Naka-cho, Koganei, Tokyo, 184-8588, Japan*

† Electronic supplementary information (ESI) available. See DOI: https://doi.org/10.1039/d5ra02051d

One approach to overcoming the limitation of high-affinity binders is to engineer the BRE to be controlled *via* an external physical or chemical signal. Indeed, there are sensing systems capable of driving reversible environmental changes that do not damage the BRE or the tissue surrounding the sensor. Several groups have identified methods to shift the local pH by 4–9 units *via* absorbing/desorbing hydrogen ions with palladium electrodes, suggesting the capability for *in vivo* pH modulation.[14–17] Acknowledging these elegant and versatile electrochemical pH modulation principles, we aimed to design an anti-insulin single chain variable fragment (scFv) with improved pH-dependent kinetics (Scheme 1). A well-documented approach to confer pH-dependent binding is through histidine mutagenesis since the p$K_a$ of histidine is near physiological pH.[18–20] Seminal translational histidine mutagenesis work outlined the development of pH-dependent therapeutic antibodies to improve their *in vivo* lifetime by decreasing their target binding ability in the acidic environment of the endosome.[21] Generating pH-dependent receptors has been reported through phage display mutagenesis, the *de novo* design of proteins, or through rational mutagenesis of proteins with available crystal structures.[22–28]

Our group previously demonstrated a proof-of-concept point-of-care insulin sensor, using an anti-insulin scFv.[29] The scFv used in this study is based on the reported HB125scFv (originally derived from the HB125IgG) in which the C-terminal sequence was compensated by sequence homology.[30] The sequence for the scFv used in the previous sensor study and present mutagenesis study is reported in Table S1,† and we will refer to it throughout the manuscript as HB125scFv-2. Due to the ability of HB125scFv-2 to detect insulin concentrations within the physiological range in a sensor format, and inspired by the success of previous histidine mutagenesis studies, we chose this scFv as an ideal candidate to improve its pH-dependent binding kinetics, although its 3D structure alone or in complex with insulin has yet to be elucidated.

In this work, we utilized protein structure prediction tools to predict the HB125scFv-2 structure complexed with insulin to identify sites for histidine mutagenesis. We used both AlphaFold 2 (AF2) combined with molecular docking simulation and AlphaFold 3 (AF3) to do so. We selected mutation sites within the complementarity-determining regions (CDRs) based on either the AF2 predicted wild-type (WT) HB125Fv-2 structure docked with human insulin (PDB: 3I40) in ClusPro 2.0 or by predicting the complexed structure using AF3.[31–34] Mutations from each model resulted in scFvs with varied pH-dependent insulin binding compared with the WT. We recombinantly prepared each histidine mutant in *Escherichia coli* (*E. coli*) and performed an initial bio-layer interferometry (BLI) screen to evaluate any loss in specificity to insulin. We then thoroughly investigated the pH-dependent binding kinetics of selected mutants to insulin in buffers at pH 7.4 and pH 6.0. Finally, we demonstrate the feasibility of using an scFv with improved pH-sensitivity as a method to improve biosensor signal regeneration with BLI.

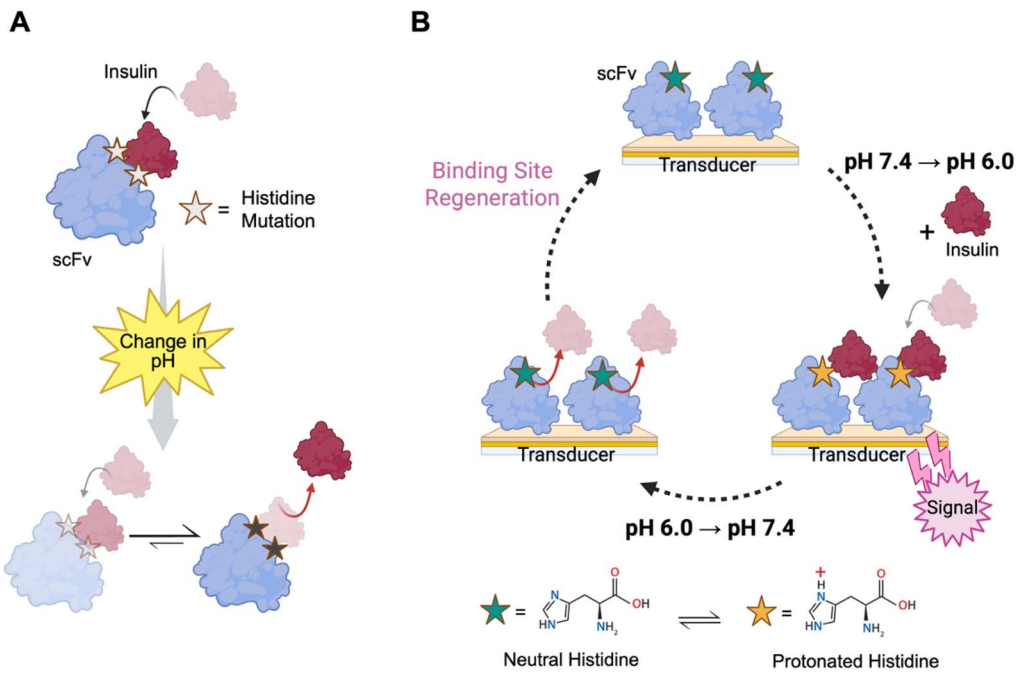


Scheme 1 Conceptual overview. (A) Improving the pH-sensitivity of an anti-insulin scFv through histidine mutagenesis allows for the selective dissociation of insulin in different pH conditions. (B) An scFv with improved pH sensitivity can be leveraged to improve biosensor regeneration through changing the local pH. This schematic shows an example where an scFv has a higher affinity for insulin when the mutated histidine is protonated and a lower affinity when neutral. In this case, only in acidic environments can an scFv immobilized on a transducer detect the binding of insulin. Conversely, through switching the pH from acidic to more neutral, dissociation of insulin allows for regeneration of the scFv binding site. Created in BioRender. Wilson, E. (2025) https://BioRender.com/piywqqe.

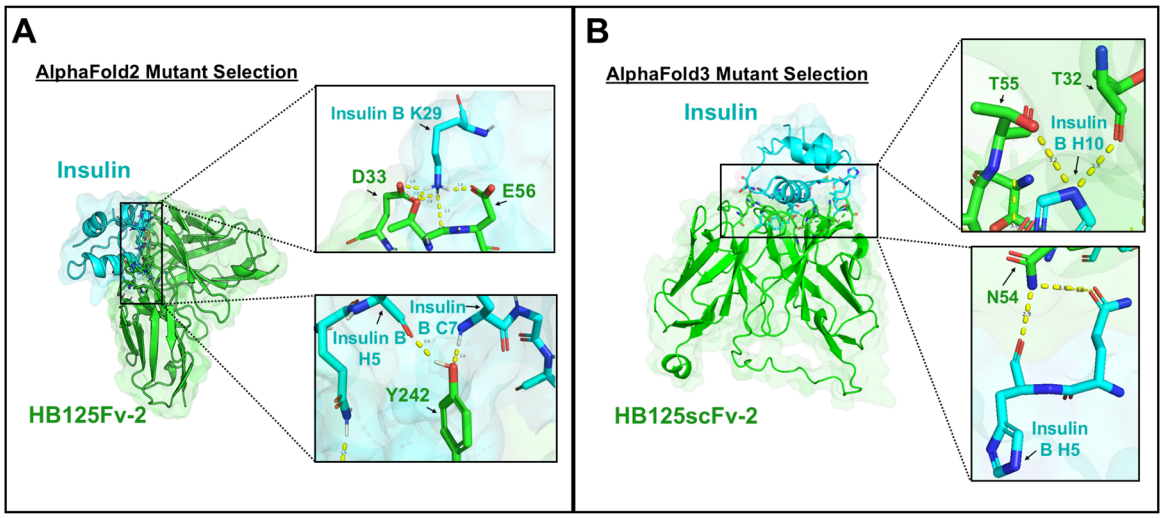


Fig. 1 Identification of potential pH-dependent mutation sites. (A) Cartoon view of the docked AlphaFold 2 wild-type HB125Fv-2 (green) with insulin (PDB: 3I40) (blue) visualized in PyMOL. Zoomed views indicate the interactions of the selected residues for mutation (D33, E56, and Y242). (B) Cartoon view of the AlphaFold 3 predicted HB125scFv-2 (green)-insulin (blue) complex visualized in PyMOL. Zoomed views indicate the interactions of the selected residues for mutation (T32, N54, and T55). All residue numbers correspond to the primary HB125scFv-2 amino acid sequence described in Table S1.†

## Results

### Design and characterization of histidine mutants

The X-ray crystal structure of HB125scFv-2 (or the parental HB125scFv or HB125IgG) alone or in complex with insulin, has not yet been experimentally determined. Therefore, we turned to computational modelling to identify residues responsible in forming the scFv complex with insulin. We input the HB125Fv-2 sequence into AF2 and docked the predicted structure with human insulin (PDB: 3I40) using the ClusPro 2.0 protein docking server in antibody mode (Fig. 1A). Our initial criteria for mutant selection centered around mutating negatively charged residues at pH 7.4 within the CDRs that interact with positively charged residues within human insulin at pH 6.0 to histidine, thereby inducing electrostatic repulsion selectively at pH 6.0. Of all the predicted polar contacts (Table S2†), only D33 and E56 were negatively charged scFv residues at neutral conditions predicted to interact with positively charged insulin residues at acidic conditions (insulin B K29). We thus selected an additional mutation site, Y242, as it is a neutral residue that is predicted to interact with multiple insulin residues, including histidine. These mutations are located within different predicted CDRs of HB125scFv-2: D33 is located within CDRH1, E56 is located within CDRH2, and Y242 is located within CDRL3 (Fig. S1†). In total, we designed three single- (D33H, E56H, Y242H), one double- (D33H/E56H) and one triple histidine mutant (D33H/E56H/Y242H) from AF2 predicted structures to assess for pH-dependent insulin binding. Then, we modeled the HB125scFv-2 complexed with insulin using AF3 (Fig. 1B). From this, we selected three additional residue sites for mutation: T32, N54, and T55. T32 flanks CDRH1 and N54 and T55 are located within CDRH2 (Fig. S1†). The additional residues selected were all predicted to interact with positively charged insulin residues under acidic conditions and were selected regardless of their charge under either condition. From the AF3 predicted structures, we designed three single- (T32H, N54H, T55H), one double- (N54H/T55H) and one triple histidine mutant (T32H/N54H/T55H). In total, we produced six single-, two double- and two triple- histidine mutants to assess for pH-dependency.

All mutants were successfully purified from the soluble fraction of *E.coli* (Fig. S2†). As all our mutations were located either within (or flanking in the case of T32) predicted CDRs, we first assessed their ability to bind to insulin. We set up a BLI sandwich assay with an anti-insulin IgG (clone C7C9) to mimic the ELISA used to confirm the specificity of the WT (Fig. S3†). BLI biosensors functionalized with the C7C9-insulin complex (Fig. S17A†) were incubated in varied concentrations of HB125scFv-2 for 10 minutes and the resultant wavelength shift after 600 seconds is plotted as a function of scFv concentration in Fig. 2 (full binding data in Fig S4†). The raw data is shown alongside a nonlinear fit of the data (see methods) solely for visualization purposes and not to derive any kinetic parameters, as neither equilibrium nor saturation are established across all assays. As we were uncertain about the extent to which each mutation affected insulin binding, we initially evaluated HB125scFv-2 concentrations ranging from 0 to 2000 nM. However, to refine our selection, we focused on mutants that exhibited specific interactions with insulin at HB125scFv-2 concentrations below 500 nM, as shown in Fig. 2B. At lower concentrations, T32H, D33H, N54H, and D33H/E56H qualitatively appeared to exhibit wavelength shifts similar to the WT, indicating a specific interaction with insulin. E56H and Y242H appear to also interact with insulin specifically, but each to a lesser extent. Notably, HB125scFv-2 mutants with the T55H mutation (T55H, N54H/T55H, and T32H/N54H/T55H) appear to

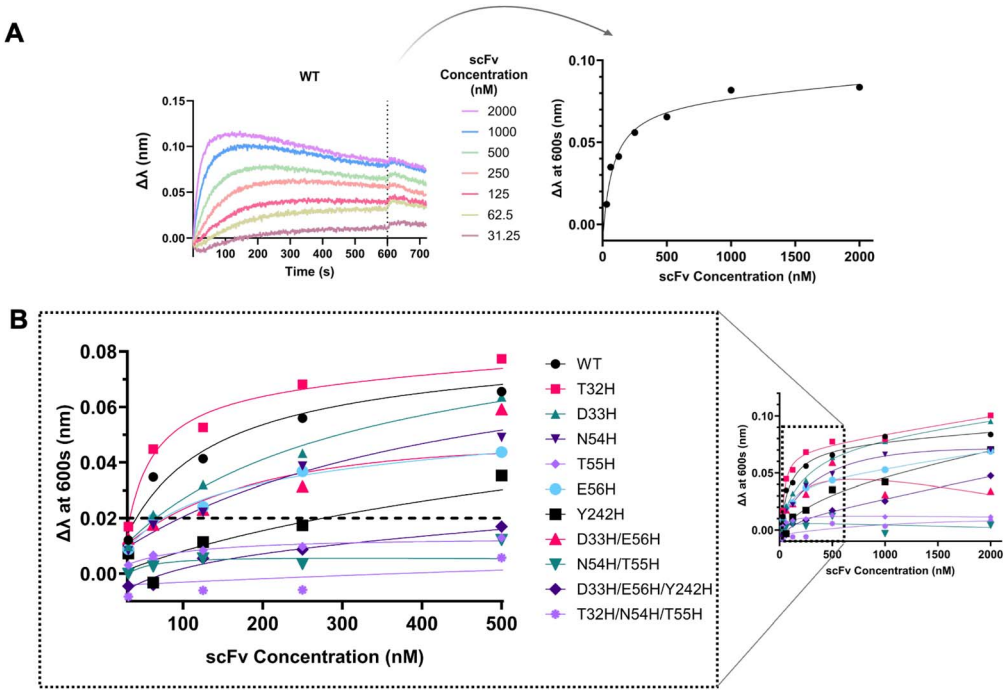


Fig. 2 Initial binding assessment of constructed histidine mutants. (A) Representative example of how the wavelength shifts for each mutant were plotted. The BLI sensorgrams for the WT are shown here. (B) Zoomed wavelength shifts at 600 seconds as a function of concentration for each HB125scFv-2 produced. Data was fit to the "One Site-Total Binding" equation (GraphPad 10.3.1) purely for visualization purposes. Full sensorgrams for each mutant are shown in Fig S4† and a schematic of the BLI assay is shown in Fig S17A.†

not interact with insulin at all in this orientation (Fig S4E, I and K†). Further studies with this mutation are necessary to understand the exact mechanism behind this apparent loss of function. Nevertheless, due to this lack of specific association from any mutant with the T55H mutation, we excluded T55H, N54H/T55H, and T32H/N54H/T55H from further screening. As these mutants all exhibited a wavelength shift of <0.02 nm at lower HB125scFv-2 concentrations, we set this as an arbitrary cutoff and thus additionally excluded D33H/E56H/Y242H from further screening. Ultimately, we selected T32H, D33H, N54H, E56H, Y242H, and D33H/E56H to move forward with an in-depth binding characterization.

### Histidine mutants exhibit variable binding in solutions of different pH

After confirming the histidine mutants were still able to bind to insulin with a sandwich assay, we set up a BLI experiment in which the WT and selected histidine mutants (T32H, D33H, N54H, E56H, Y242H, D33H/E56H) were immobilized directly on the sensor surface using amine coupling (Fig. S17B†). We then quantified the kinetic parameters of each mutant by evaluating binding across multiple insulin concentrations in both buffers at pH 7.4 and pH 6.0 across three independent experiments to account for the batch-to-batch variability of biosensor functionalization and protein preparations. While we initially hypothesized these mutations to histidine would result in electrostatic repulsion between HB125scFv-2 and insulin selectively at pH 6.0, kinetic data suggest these histidine mutations were not sufficient to overcome the inherent pH-dependency of the WT (Fig. 3 and Table 1). All scFvs exhibit a stronger association with insulin at pH 6.0, as the ratios of average $K_D$ values at pH 7.4 to 6.0 of the scFvs are all greater than 1. However, some mutants such as, D33H, N54H, and the double D33H/E56H mutant have reduced the pH-dependency of the WT as seen in the decreased average $K_D$ ratio compared to the WT.

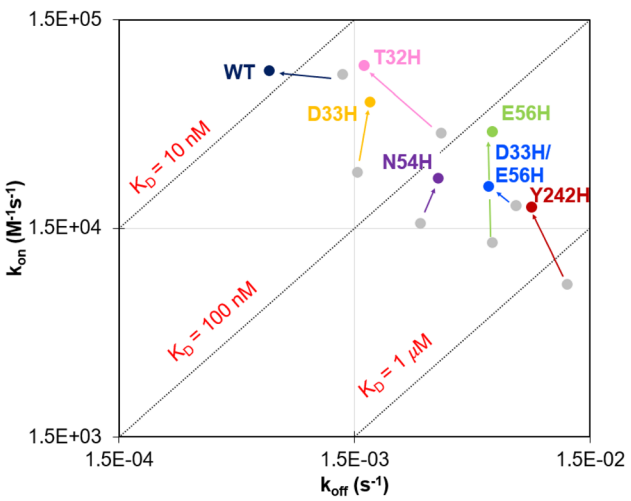


Fig. 3 Iso-affinity plots of histidine mutants at pH 7.4 and pH 6.0. Binding data were recorded at pH 7.4 (gray dots) and at pH 6.0 (colored dots) across six concentrations of insulin for all scFvs. $K_D$, $k_{on}$, and $k_{off}$ values are reported as the average estimates of $N = 3$ independent BLI assays and are displayed in Table 1. The full BLI binding traces for each mutant are displayed in Fig. S5–S11.†

Table 1 Kinetic parameters of histidine mutants derived from amine-coupled BLI assays. $K_D$, $k_{on}$, and $k_{off}$ values are reported as the average ± standard deviation estimates of $N = 3$ independent BLI assays

| | pH 7.4 | | | pH 6.0 | | | Average $K_D$ ratio (pH 7.4/6.0) | Average fold change from WT |
|---|---|---|---|---|---|---|---|---|
| scFv | $k_{on}$ ($M^{-1}$ $s^{-1}$) | $k_{off}$ ($s^{-1}$) | $K_D$ (nM) | $k_{on}$ ($M^{-1}$ $s^{-1}$) | $k_{off}$ ($s^{-1}$) | $K_D$ (nM) | | |
| WT | 81 418 ± 2353 | 0.00134 ± 0.00011 | 16.4 ± 1.3 | 85 017 ± 5112 | 0.00066 ± 0.00019 | 7.4 ± 1.9 | 2.2 | — |
| T32H | 42 935 ± 12 322 | 0.00351 ± 0.00060 | 145.5 ± 83.1 | 89 714 ± 7107 | 0.00166 ± 0.00058 | 17.4 ± 5.1 | 8.4 | 3.8 |
| D33H | 27 774 ± 5836 | 0.00154 ± 0.00059 | 51.7 ± 15 | 60 477 ± 15 234 | 0.00176 ± 0.00007 | 36 ± 10.6 | 1.4 | 0.6 |
| N54H | 15 703 ± 2810 | 0.00286 ± 0.00012 | 206 ± 51 | 25 978 ± 7349 | 0.00341 ± 0.00024 | 165.3 ± 45.2 | 1.2 | 0.6 |
| E56H | 12 712 ± 3163 | 0.00577 ± 0.00037 | 547.7 ± 141.7 | 43 414 ± 6123 | 0.00580 ± 0.00163 | 160.4 ± 71.6 | 3.4 | 1.5 |
| Y242H | 8036 ± 515 | 0.01205 ± 0.002 | 1479.7 ± 193.7 | 18 848 ± 2014 | 0.00854 ± 0.00099 | 477.6 ± 89.6 | 3.1 | 1.4 |
| D33H/ E56H | 19 136 ± 3444 | 0.0073 ± 0.00118 | 426.1 ± 117.6 | 23 695 ± 2578 | 0.00557 ± 0.00061 | 250.4 ± 52.7 | 1.7 | 0.8 |

The mutations resulted in scFvs with apparent $K_D$ values between 3- and 90-times greater than the WT at pH 7.4. However, the T32H mutant exhibits a strong association with insulin at pH 6.0, comparable to the WT at pH 7.4. The $K_D$ of the T32H mutant is calculated to be 145.5 ± 83.1 nM at pH 7.4 and 17.4 ± 5.1 nM at pH 6.0 – an average of an 8.4× difference between the two conditions, and a 3.8× increase in pH-sensitivity from the WT. The iso-affinity plot of the kinetic data of T32H (Fig. 3, pink dot) suggests that this is due to both $k_{on}$ and $k_{off}$ contributions. In comparison, the pH-dependency of the WT is largely driven by changes in $k_{off}$ (Fig. 3, navy dot). Furthermore, the derived $k_{on}$ and $k_{off}$ values of the T32H mutant at pH 6.0 closely align with those of the WT at pH 7.4, suggesting a high specificity to insulin at that pH condition. We thus moved forward with only evaluating T32H compared to the WT.

### Evaluation of pH-responsiveness in fluctuating insulin concentrations with BLI under isocratic and dynamic pH conditions

We next investigated the ability of both the T32H mutant and the WT to measure successive, and rapidly changing concentrations of insulin under isocratic pH conditions. We designed a BLI assay in which we quickly (60 s) established the association phase in stepwise increasing and decreasing concentrations of insulin (0.5–2 μM) with a 60 s dissociation phase between each insulin concentration (Fig. 4A and B). The buffer pH for all assays remained unchanged and the BLI sensor functionalization is shown in Fig. S17B.† To quantify the impact of pH on sensor regeneration, we analyzed the percentage of relative binding and unbinding which occurred upon each subsequent step. Fig. 4C explains how we calculated this percentage change. As there is direct correlation between scFv

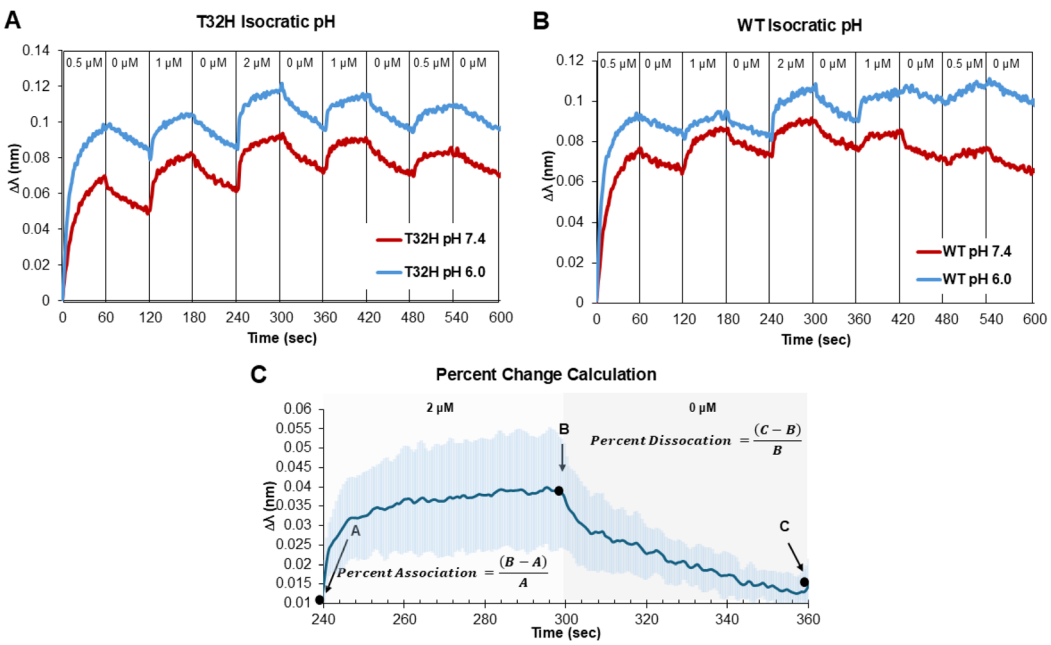


Fig. 4 Time course BLI signal response of T32H and WT HB125scFv-2 to varying insulin concentrations (0–2 μM) under isocratic pH conditions at either pH 7.4 or 6.0. (A) Wavelength shift (nm) of T32H at pH 7.4 (red) and at pH 6.0 (blue). (B) Wavelength shift (nm) of the WT at pH 7.4 (red) and at pH 6.0 (blue). (C) Representative example of percent change calculation for each association and dissociation step.

Table 2 Percent change of association and dissociation cycles for T32H and WT HB125scFv-2 under isocratic pH conditions

| | T32H pH 7.4 | T32H pH 6 | WT pH 7.4 | WT pH 6 |
|---|---|---|---|---|
| **Association** | | | | |
| 0.5 μM → 1 μM | 57% | 31% | 29% | 15% |
| 1 μM → 2 μM | 49% | 39% | 24% | 32% |
| 2 μM → 1 μM | 21% | 20% | 6% | 11% |
| 1 μM → 0.5 μM | 23% | 15% | 7% | 8% |
| **Dissociation** | | | | |
| 0.5 μM → 0 μM | −22% | −18% | −12% | −12% |
| 1 μM → 0 μM | −23% | −15% | −16% | −12% |
| 2 μM → 0 μM | −20% | −21% | −15% | −13% |
| 1 μM → 0 μM | −22% | −18% | −15% | −5% |
| 0.5 μM → 0 μM | −17% | −11% | −11% | −9% |
| **Average association** | 37% | 26% | 16% | 17% |
| **Average dissociation** | −21% | −17% | −14% | −10% |

fraction bound and wavelength shift, we took the difference between initial wavelength shift (pre-association, point A) as well as the final wavelength shift (post-association, point B) as the change in fraction bound over each 60 seconds step. This change was then normalized to the initial wavelength shift (point A), giving a ratio corresponding to the relative change in bound or unbound scFv. These ratios are reported as percentage changes across each increasing and decreasing insulin concentration at both pH values for both T32H and the WT HB125scFv-2 in Table 2.

An example to provide context for these values is as follows: when a BLI sensor functionalized with T32H is allowed to dissociate in 0 μM insulin at pH 7.4 after association with 0.5 μM insulin at pH 7.4, the sensor signal decreases by 22% compared to the WT signal decrease of 12% under the same conditions. This shows that over the 60 seconds dissociation period, T32H regenerated relatively 10% more binding sites when compared to WT, or had relatively 10% less scFv bound complex. Using this metric, we can compare the average association and dissociation responses across each cycle. On average, the T32H mutant was more responsive to increasing insulin concentrations at pH 7.4 (37%) than at pH 6.0 (26%), whereas the WT response during insulin association was similar at pH 7.4 (16%) and at pH 6.0 (17%). The dissociation signals were comparable between T32H and the WT, with an average increase of about 4% between pH 7.4 and pH 6.0 for both scFvs. To further interrogate the pH-dependent kinetics of each HB125scFv-2, we created insulin-dependent calibration curves with these relative association and dissociation signals (Fig. S13†) and evaluated the transient BLI shift (Fig. S12†) by taking the empirical time derivative for each signal. The T32H mutant shows a strong insulin-dependent response at pH 6.0 for increasing insulin concentrations compared to pH 7.4 where there is poor correlation between signal and concentration (Fig. S14†). The change in transient response of the WT HB125scFv-2 between the two pH conditions is much more subtle. Although both scFvs exhibit a stronger association to insulin in pH 6.0, these results, along with the derived kinetic parameters, suggest the T32H mutant is more sensitive to changes in pH than the WT.

As the T32H mutant exhibited the largest change in binding affinity between the two pH conditions, we challenged its ability to detect increasing and decreasing concentrations of insulin compared to the WT in fluctuating pH conditions. We designed a BLI assay (Fig. S17B†) in which the association phase occurred in buffer at pH 6.0 for 60 seconds and the dissociation phase occurred in buffer at pH 7.4 for 60 seconds. We repeated this cycle across a stepwise increase and decrease of insulin concentrations ranging from 0.5–2 μM. Fig. 5A displays the average wavelength shifts and standard deviation for triplicate sensors functionalized with either the T32H mutant (blue line) or the WT (red line). To help account for variability in HB125scFv-2 density on each BLI probe, Fig. 5B shows the same results, but normalized to the first association step of 0.5 μM insulin. To further compare the kinetics between the T32H mutant with the WT, transient wavelength shifts were calculated (Fig. S15†). The T32H mutation shows larger transient changes compared to the WT. The transient changes plotted as a function of insulin concentration also demonstrate the improved pH-sensitivity of the T32H mutant (Fig. S16†). We report the percentage change as described in Fig. 4C for each association and dissociation cycle, excluding the initial association in Fig. 5C and D. The percentage change for the T32H mutant in dynamic pH conditions is significantly greater compared to the WT. This trend is apparent in both the association and dissociation response, showing a statistically significant difference in every fluctuation of insulin other than dissociation from 2–0 μM. As we can correlate this relative percent change to the shift in bound or unbound scFv complex over 60 seconds, these results demonstrate the single histidine mutation improves the pH sensitivity compared to the WT and allows for greater sensor regeneration under dynamic pH conditions.

## Discussion

In this study, we report the design and construction of various histidine mutations within an anti-insulin scFv, referred to as HB125scFv-2, that we previously used to develop a point-of-care insulin sensor. We designed these mutants with translation in mind and envisioned our mutant would be integrated with existing technology capable of modulating the pH of an electrode electrochemically. Indeed, the selective modulation of receptor–ligand binding is a powerful tool in many areas of biotechnology and particularly in the development of biosensors. Generally, the capacity to trigger a change in the kinetics of a high-affinity biological recognition element, such as an antibody, is necessary to facilitate reliable, continuous quantification of biomarkers present at low concentrations. Therefore, we aimed to engineer the directed reversibility of the scFv through a change in pH.

We utilized AF2- and AF3- predicted structures as a starting point to guide our mutagenesis. From the predicted interactions between the WT HB125scFv-2 and insulin (Table S2†), we selected mutation sites we hypothesized would introduce

 

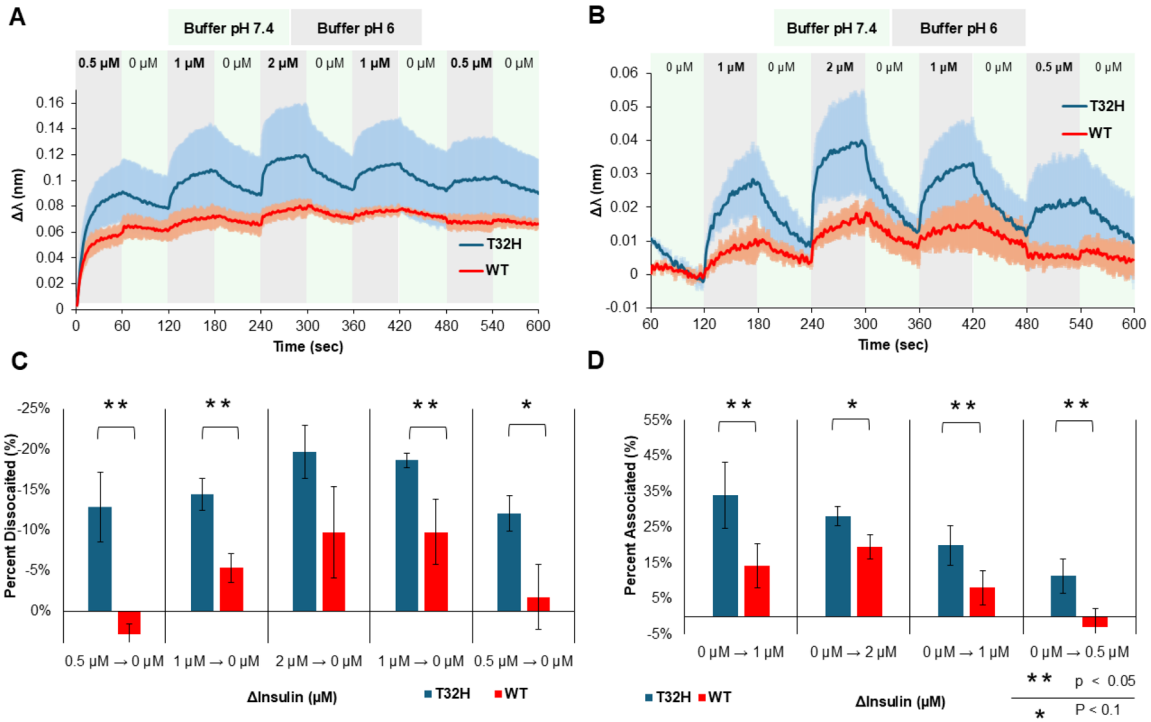


Fig. 5 Evaluation of binding site regeneration with BLI under dynamic pH conditions with T32H and WT. (A) Average wavelength shifts for triplicate sensors functionalized with T32H (blue) and the WT (red) in response to increasing and decreasing insulin concentrations. Insulin association was recorded in buffer at pH 6.0 while dissociation was recorded in buffer at pH 7.4. (B) Wavelength shifts reported in (A) normalized to first association step. Average and standard deviation of (C) percent dissociation and (D) percent association across each insulin cycle. Stars denote statistical significance calculated from a paired sample *t*-test ($p < 0.05$ denoted by two stars, and $p < 0.1$ denoted by a single star).

electrostatic repulsions specifically at pH 6.0. Upon experimental validation of these mutants, it became clear that the mutation sites selected were not sufficient in overcoming the inherent pH-dependency of the WT. In our case, we were able to obtain mutants with varied pH-sensitivity, however it remains a challenge to computationally predict the functional effects of potential point mutations. A clear example of this challenge is present in this work: both T32 and T55 were predicted with AF3 to interact with insulin B H10. One mutation appeared to eliminate the specificity to insulin (T55H) whereas one mutation increased the pH-sensitivity (T32H).

Through quantifying the kinetic parameters of each mutant at pH 7.4 and pH 6.0, we identified T32H as the mutation with the greatest difference in insulin binding between the two conditions. We used BLI to quantitatively asses the kinetic parameters in triplicate to help account for differences in batch-to-batch variability found in the fabrication processes, as subtle differences in receptor density can lead to different calculated $K_D$ values.[35] Through evaluating the response of T32H to increasing and decreasing insulin concentrations in static pH conditions, it appeared that this mutation resulted in an HB125scFv-2 with increased pH-sensitivity compared to the WT. As outlined in Table 2, at static pH conditions (both pH 7.4 and pH 6.0), T32H exhibited a greater percent change in wavelength shift compared to the WT across each increasing and decreasing insulin concentration, a metric correlated to the change in the scFv-insulin complex. These results highlight the greater pH-dependent response the T32H mutant has compared to WT, especially during association. Notably, this led to T32H mutant producing an overall greater signal.

Based on the increased pH-sensitivity of the T32H mutant, we designed a BLI assay to interrogate how a sensor would respond in dynamic insulin concentrations and dynamic pH conditions. We repeated stepwise increasing and decreasing concentrations of insulin where the association phase occurred in buffer at pH 6.0 and the dissociation phase occurred in buffer at pH 7.4. This assay was designed to understand if the increased pH-sensitivity of the T32H mutant would improve binding site regeneration, as the dynamic pH conditions were utilized to simulate the application of an external signal to induce dissociation. The results from this assay, as outlined in Fig. 5C and D support the idea that improved pH-sensitivity can be leveraged to improve biosensor regeneration. Taken together, these results show promise for exploiting an anti-insulin scFv with improved pH-sensitivity in an *in vivo* continuous biosensing system with the combination of electrochemical pH modulation principles and/or electrochemical or optical detection methods.

Translation of this research involves detecting physiologically-relevant insulin concentrations. While the physiological range of insulin varies among nondiabetic individuals, as well as patients with type 1 and type 2 diabetes, depending on patient-specific insulin sensitivity and dosage requirements, plasma insulin levels rarely approach nanomolar

concentrations in blood.[36–38] While the T32H mutation exhibited the largest pH-sensitivity, the lowest $K_D$ values for both the WT and T32H are greater than 10 nM, and therefore will have very low occupancy at the physiological range of insulin. We previously demonstrated that by leveraging faradaic electrochemical impedance spectroscopy (EIS), a transduction technique sensitive enough to measure small changes in binding, we can detect physiologically-relevant insulin concentrations with HB125scFv-2. However, further efforts to improve the scFv sensitivity and develop/combine more feasible detection principles for *in vivo* use may be required to measure interactions between a BRE and substrate at much lower concentrations than the expected $K_D$.[39,40] Beyond engineering of the scFv, there are several aspects to consider prior to integration into an electrochemical sensor. These considerations include the stable immobilization of the scFv, reliable signal transduction upon binding, sensor specificity, and the ability to locally shift pH substantially to enable rapid dissociation and association of insulin. Integration of an scFv onto an electrode has been demonstrated by several groups, leading to a stable, self-assembled monolayer for both *in vitro*, and *in vivo* applications.[41] Coupling the scFv immobilization with soft lithography patterning of palladium electrodes is a potential avenue to translate this research into a compatible electrochemical platform.[14,42,43] Furthermore, the ability to measure the specific and real-time association and dissociation of the scFv and insulin electrochemically in complex sample matrices is key to the translation of this research.[44,45] There are several methods being developed for the rapid, and real-time detection of interactions between BREs and substrates utilizing extended gate field effect transistors or EIS, which can measure changes in the localized charge or capacitance of the electrode surface, respectively.[46,47]

The engineering of BREs is a key approach to facilitate the development of the continuous *in vivo* monitoring of proteins/peptides, since biosensor performance is strongly dependent on the characteristics of BREs. In addition, alternate approaches to meet the analytical requirements for *in vivo* biosensing have been reported. Novel algorithms and systems have been developed to enhance sensitivity by either extending the dynamic range through tuning the apparent $K_D$ based on system geometry or by measuring true substrate concentration independently of kinetics through pre-equilibrium.[48–53] Although these methods are highly innovative and have created new opportunities, several practical limitations still exist, such as the use of homogeneous reporters or the assumption of only reaction-limited responses. These conditions are very challenging to maintain *in vivo*, where the BRE is immobilized on a sensor surface. The system may also experience changes in mass transport properties over time due to the immune response.[54–56] However, a recently published technique in which high-frequency oscillation is used to induce dissociation is an elegant approach to overcome the limitations of high-affinity BREs.[57] This recent research work circumvents engineering the BRE by finding a specific external stimulus to apply that still induces dissociation. The combination of these innovative algorithms and techniques with our engineered BRE will circumvent current challenges in the *in vivo* continuous monitoring of proteins and peptides.

# Conclusions

We engineered an anti-insulin scFv with improved pH-sensitivity through histidine mutagenesis guided by predicted structures and interactions. We thoroughly quantified the impact of the histidine mutations both in the measured kinetic values, as well as demonstrated the ability to use pH-dependent kinetics for tracking changes in insulin concentrations with BLI. This work showcases the feasibility of using histidine mutagenesis to engineer BREs as a method to overcome limitations in continuous monitoring. Future experimentation will explore translation of the selective binding of the T32H mutant as a strategy to further improve biosensor regeneration.

# Materials and methods

### Chemicals

Sodium chloride, potassium chloride, sodium phosphate dibasic, potassium phosphate monobasic, imidazole, isopropyl ß-D-1-thiogalactopyranoside (IPTG) and kanamycin were all purchased from Millipore Sigma (Burlington, MA, USA). Anti-insulin monoclonal antibody C7C9, Tween 20, yeast extract, were purchased from Fisher Scientific (Hampton, NH, USA). Bovine serum albumin (BSA, 2 mg per mL solution) and peptone 140 were purchased from Avantor/VWR (Radnor, PA, USA).

### Structural prediction

The structure of the anti-insulin HB125Fv-2 was predicted using the primary sequence of the HB125scFv[30] and input intoAlphaFold 2 *via* ColabFold (**https://colab.research.google.com/github/sokrypton/ColabFold/blob/main/AlphaFold2.ipynb**). The lowest ranked model was input into the Cluspro 2.0 docking server as the receptor. The deposited PBD file of human insulin (PDB: 3I40) was input as the ligand. Antibody mode was selected, and we indicated to "Automatically Mask non-CDR regions." The lowest ranked output of protein–protein docking was visualized in PyMOL Version 2.5 (Schrödinger Inc., New York, USA), and predicted hydrogen bonds were viewed with the "Show Contacts" Plugin. For AlphaFold 3 predictions, the sequence of the WT HB125scFv-2 and Insulin were input as separate proteins into the AlphaFold Server (**https://alphafoldserver.com/**). The lowest ranked output was visualized in PyMOL and predicted hydrogen bonds were viewed with the "Show Contacts" Plugin.

### Cloning, protein expression, and purification

The scFv used in this study, designated as HB125scFv-2 is based on the reported HB125scFv, in which the C-terminal sequence was compensated by sequence homology (sequence data in Table S1†). This scFv is specific to insulin, with an apparent $K_D$ as determined by an enzyme-linked immunosorbent assay (ELISA) of 6 nM (Fig. S3†). Codon-optimized WT and putative

pH-sensitive mutant scFv genes were designed and synthesized into a pet30c(+) expression vector (GenScript, Piscataway, NJ, USA). All scFvs used in this study were expressed and purified with the protocol that follows. Plasmids were transformed into *Escherichia coli* (*E. coli*) *SHuffle T7 Express Competent* cells (New England Biolabs; Ipswich, MA, USA) according to the manufacturer's protocol. A mixture of transformants was inoculated into 3 mL of Luria-Bertani (LB) media supplemented with 50 μg per mL kanamycin for 24 hours at 28 °C. One percent of preculture (% v/v) was inoculated into 10 flasks, each containing 100 mL of LB Media supplemented with 50 μg per mL kanamycin. Cultures were grown at 37 °C with 200 rpm shaking until the $OD_{600}$ reached ~0.4–0.6 (typically 3–5 hours). Protein expression was induced with 100 μM IPTG for 12 hours at 16 °C with 170 rpm shaking. Cells were resuspended in purification buffer (20 mM potassium phosphate, pH 7.4, 500 mM NaCl, 20 mM imidazole) and lysed mechanically *via* French Pressure (Glen Mills) twice (2000psi, 30 seconds each). Following centrifugation (10 000×*g* 10 minutes, 4 °C) and ultracentrifugation (145 000×*g* 1 hour, 4 °C), the clarified cell lysate was purified *via* nickel affinity chromatography (Histrap 1 mL, Cytiva; elution buffer: 20 mM potassium phosphate, pH 7.4, 500 mM NaCl, 500 mM imidazole) on an Äkta Pure Fast Performance Liquid Chromatography (Cytiva; Marlborough, MA) system. Fractions containing the protein of interest as determined by SDS Page were pooled and dialyzed to phosphate-buffered saline (pH 7.4, 137 mM NaCl, 2.7 mM KCl, 8 mM $Na_2HPO_4$, and 2 mM $KH_2PO_4$). The buffer-exchanged sample was further purified *via* gel filtration (Superdex 200 increase 10/300 GL column, Cytiva). Eluted fractions were analyzed by SDS Page and protein concentration was determined by a DC Protein Assay (BioRad; Hercules, CA, USA). Samples were pooled, concentrated, and stored at −80 °C until use.

### Biolayer interferometry (sandwich assay)

Anti-mouse Fc capture (AMC) Biosensors (Sartorius; Göttingen, Germany) were equilibrated in BLI running buffer (phosphate-buffered saline, pH 7.4, 0.005% v/v Tween 20, 1% v/v BSA) for at least 10 minutes prior to use. All BLI runs were performed on an Octet R2 System (Sartorius) at a temperature of 23 °C with shaking at 700 rpm. Following a 30 seconds initial baseline, 12.5 mg $mL^{-1}$ of anti-insulin IgG clone C7C9 was immobilized onto the AMC sensor tips. Biosensors were re-equilibrated for 30 seconds and 10 μM insulin was loaded onto the tips for 300 seconds. A saturating concentration of insulin was used to ensure the binding interaction was solely dependent on the interaction of the scFv with insulin. Following another 30 seconds baseline, loaded biosensors were incubated in varied concentrations of either WT or mutant scFv for 600 seconds to establish to association phase. Dissociation traces were recorded in BLI running buffer for 120 seconds. Eight concentrations of scFv were used for each run, and each run included a reference for subtraction of non-specific binding. To visualize the specificity of each scFv, the wavelength shift at 600 seconds was plotted as a function of concentration. Data was fit to the "One Site-Total Binding" equation (GraphPad 10.3.1; GraphPad Sofware LLC, Boston, MA, USA) purely for visualization purposes, as neither equilibrium nor saturation are established across all conditions.

### Biolayer interferometry for derivation of kinetic parameters

Amine-Reactive Generation 2 Biosensors (AR2G) Biosensors (Sartorius) were equilibrated in MQ for at least 10 minutes prior to use. All BLI runs were performed on an Octet R2 System (Sartorius) at a temperature of 30 °C with shaking at 700 rpm. Following a 30 seconds initial baseline in MQ, sensor tips were activated with a 20 mM : 10 mM EDC : NHS solution for 300 seconds. Activated sensors were loaded with 20 μg per mL scFv diluted in 10 mM acetate buffer pH 6.0 for 600 seconds. Sensors were quenched in 1 M ethanolamine for 300 seconds following scFv loading. Then, sensors were equilibrated in BLI running buffer (phosphate-buffered saline, pH 7.4, 0.005% v/v Tween 20, 1% v/v BSA either pH 7.4 or pH 6.0) for 120 seconds to establish a baseline. Following the baseline, loaded biosensors were incubated in varied concentrations of insulin for 120 seconds to establish the association phase. Dissociation traces were recorded in BLI running buffer for 180 seconds. The running buffer was kept the same throughout the assay (either 7.4 or 6.0), and each run included a reference (scFv immobilized, but no insulin added) for subtraction of non-specific binding. Nonlinear regression analysis was performed Graphpad Prism 10.2.3 using the built-in "Association then Dissociation" function (reproduced below) to derive kinetic parameters.

$$K_{OB} = [\text{Radioligand}] \times k_{on} + k_{off}$$

$$K_D = \frac{k_{off}}{k_{on}}$$

$$E_q = \frac{B_{max} \times \text{Radioligand}}{(\text{Radioligand}) + K_D}$$

$$\text{Association} = E_q \times (1 - e^{(-1 \times K_{OB} \times X)})$$

$$Y \text{ at time}_0 = E_q \times (1 - e^{(-1 \times K_{OB} \times \text{time}_0)})$$

$$\text{Dissociation} = Y \text{ at time}_0 \times e^{(-1 \times k_{off} \times (X - \text{time}_0))}$$

$$Y = \text{IF}(X < \text{time}_0, \text{association}, \text{dissociation}) + \text{NS}$$

where: $k_{on}$ and $k_{off}$ are shared between all datasets, $B_{max}$ = maximum binding at equilibrium with maximum concentration of radioligand, NS = signal baseline during unbinding $X$ = time elapsed, $\text{time}_0$ = time at which dissociation was initiated.

### Bio-layer interferometry to interrogate pH-responsiveness of the T32H and WT scFvs

**All assays started with this protocol.** Amine-Reactive Generation 2 Biosensors (AR2G) Biosensors (Sartorius) were

equilibrated in MQ for at least 10 minutes prior to use. All BLI runs were performed on an Octet R2 System (Sartorius) at a temperature of 30 °C with shaking at 700 rpm. Following a 30 seconds initial baseline in MQ, sensor tips were activated with a 20 mM : 10 mM EDC : NHS solution for 300 seconds. Activated sensors were loaded with 20 μg per mL scFv diluted in 10 mM acetate buffer pH 6.0 for 600 seconds. Sensors were quenched in 1 M ethanolamine for 300 seconds following scFv loading.

**For assays in which insulin concentrations varied, but the pH remained the same.** Following scFv functionalization, sensors were equilibrated in BLI running buffer (phosphate-buffered saline, pH 7.4, 0.005% v/v Tween 20, 1% v/v BSA either pH 7.4 or pH 6.0) for 120 seconds to establish a baseline. Following the baseline, loaded biosensors were incubated in varied concentrations of insulin for 60 seconds in the same baseline buffer to establish the association phase. Dissociation traces were recorded in BLI running buffer (the same pH as the initial condition) for 60 seconds. Each run included a reference (scFv immobilized, but no insulin added) for subtraction of non-specific binding.

**For assays in which insulin concentrations varied, but the pH switched.** Following scFv functionalization, sensors were equilibrated in BLI running buffer (phosphate-buffered saline, pH 7.4, 0.005% v/v Tween 20, 1% v/v BSA pH 6.0) for 120 seconds to establish a baseline. Following the baseline, loaded biosensors were incubated in varied concentrations of insulin for 60 seconds in BLI running buffer at pH 6.0 to establish the association phase. Dissociation traces were recorded in BLI running buffer pH 7.4 for 60 seconds. Each run included a reference (scFv immobilized, but no insulin added) for subtraction of non-specific binding and to account for the jump in signal when switching between pH conditions.

All raw binding traces were filtered with the built-in Savitzky–Golay filter in the Octet Analysis Studio 13.0.

## Ethical statement

EDW, RA, and KS filed a report of invention (24-0056) related to this work to the University of North Carolina at Chapel Hill on Dec. 13, 2024, and filed a U.S. Provisional Patent Application (No. 63/784,675) on April 7, 2025.

## Data availability

The data supporting the conclusions of this work are found in the manuscript as well as the ESI.†

## Author contributions

Ellie D. Wilson: conceptualization; investigation; writing – original draft; methodology; validation; writing – review and editing; formal analysis; data curation. David Probst: investigation; writing – original draft; formal analysis; data curation, writing – review and editing. Mai Hamasaki: conceptualization; investigation; methodology. Miho Oda: conceptualization; investigation; methodology. Varun Kochar: investigation; methodology. Qianming Xu: conceptualization; investigation; methodology. Ayumi Tanaka: investigation; methodology. Hirobumi Suzuki: investigation; methodology. Ryutaro Asano: conceptualization; funding acquisition; writing – original draft; writing – review and editing; validation; methodology; formal analysis; project administration; supervision; resources. Koji Sode: conceptualization; funding acquisition; writing – original draft; writing – review and editing; validation; methodology; formal analysis; project administration; supervision; resources.

## Conflicts of interest

The authors declare no other competing interests.

## Acknowledgements

This work was financially supported by The Leona M. and Harry B. Helmsley Charitable Trust foundation, Grant ID: 2308-06273, as well as the Lampe Joint Department of Biomedical Engineering between the University of North Carolina at Chapel Hill and North Carolina State University. The authors would like to express their gratitude to Dr Bryant J. Kane for his assistance in the editing process and Dr Michael Daniele and Dr Jeffrey T. La Belle for their experimental advice.

## References

1 P. V. Röder, B. Wu, Y. Liu and W. Han, *Exp. Mol. Med.*, 2016, **48**, e219.
2 American Diabetes Association, *Diabetes Care*, 2014, **37**, S81–S90.
3 S. H. Golden and T. Sapir, *J. Manag. Care Pharm.*, 2012, **18**, 1–17.
4 D. De Pereda, S. Romero-Vivo, B. Ricarte, P. Rossetti, F. J. Ampudia-Blasco and J. Bondia, *Comput. Methods Biomech. Biomed. Eng.*, 2016, **19**, 934–942.
5 N. Poolsup, N. Suksomboon and A. M. Kyaw, *Diabetol. Metab. Syndr.*, 2013, **5**, 39.
6 E. Vargas, P. Nandhakumar, S. Ding, T. Saha and J. Wang, *Nat. Rev. Endocrinol.*, 2023, **19**, 487–495.
7 R. Soffe, V. Nock and J. G. Chase, *ACS Sens.*, 2019, **4**, 3–19.
8 J. Kim, A. S. Campbell, B. E.-F. De Ávila and J. Wang, *Nat. Biotechnol.*, 2019, **37**, 389–406.
9 S. S. Gambhir, T. J. Ge, O. Vermesh, R. Spitler and G. E. Gold, *Sci. Transl. Med.*, 2021, **13**, eabe5383.
10 D. C. Klonoff, D. Ahn and A. Drincic, *Diabetes Res. Clin. Pract.*, 2017, **133**, 178–192.
11 I. Lee, D. Probst, D. Klonoff and K. Sode, *Biosens. Bioelectron.*, 2021, **181**, 113054.
12 C. D. Flynn, D. Chang, A. Mahmud, H. Yousefi, J. Das, K. T. Riordan, E. H. Sargent and S. O. Kelley, *Nat. Rev. Bioeng.*, 2023, **1**, 560–575.
13 E. Wilson, D. Probst and K. Sode, *Appl. Phys. Rev.*, 2023, **10**, 041309.
14 C. Sharkey, J. Twiddy, K. L. Peterson, A. F. Aroche, S. Menegatti and M. A. Daniele, in *2023 IEEE BioSensors Conference (BioSensors)*, IEEE, London, United Kingdom, 2023, pp. 1–4.

15 X. Strakosas, J. Selberg, P. Pansodtee, N. Yonas, P. Manapongpun, M. Teodorescu and M. Rolandi, *Sci. Rep.*, 2019, **9**, 10844.
16 Y. Deng, T. Miyake, S. Keene, E. E. Josberger and M. Rolandi, *Sci. Rep.*, 2016, **6**, 24080.
17 Z. Hemmatian, S. Keene, E. Josberger, T. Miyake, C. Arboleda, J. Soto-Rodríguez, F. Baneyx and M. Rolandi, *Nat. Commun.*, 2016, **7**, 12981.
18 M. L. Murtaugh, S. W. Fanning, T. M. Sharma, A. M. Terry and J. R. Horn, *Protein Sci.*, 2011, **20**, 1619–1631.
19 C. Schröter, R. Günther, L. Rhiel, S. Becker, L. Toleikis, A. Doerner, J. Becker, A. Schönemann, D. Nasu, B. Neuteboom, H. Kolmar and B. Hock, *mAbs*, 2015, **7**, 138–151.
20 C. A. Sarkar, K. Lowenhaupt, T. Horan, T. C. Boone, B. Tidor and D. A. Lauffenburger, *Nat. Biotechnol.*, 2002, **20**, 908–913.
21 T. Igawa, S. Ishii, T. Tachibana, A. Maeda, Y. Higuchi, S. Shimaoka, C. Moriyama, T. Watanabe, R. Takubo, Y. Doi, T. Wakabayashi, A. Hayasaka, S. Kadono, T. Miyazaki, K. Haraya, Y. Sekimori, T. Kojima, Y. Nabuchi, Y. Aso, Y. Kawabe and K. Hattori, *Nat. Biotechnol.*, 2010, **28**, 1203–1207.
22 H. Watanabe, H. Matsumaru, A. Ooishi, Y. Feng, T. Odahara, K. Suto and S. Honda, *J. Biol. Chem.*, 2009, **284**, 12373–12383.
23 J. S. Harrison, C. D. Higgins, M. J. O'Meara, J. F. Koellhoffer, B. A. Kuhlman and J. R. Lai, *Structure*, 2013, **21**, 1085–1096.
24 P. Bonvin, S. Venet, G. Fontaine, U. Ravn, F. Gueneau, M. Kosco-Vilbois, A. E. Proudfoot and N. Fischer, *mAbs*, 2015, **7**, 294–302.
25 S. E. Boyken, M. A. Benhaim, F. Busch, M. Jia, M. J. Bick, H. Choi, J. C. Klima, Z. Chen, C. Walkey, A. Mileant, A. Sahasrabuddhe, K. Y. Wei, E. A. Hodge, S. Byron, A. Quijano-Rubio, B. Sankaran, N. P. King, J. Lippincott-Schwartz, V. H. Wysocki, K. K. Lee and D. Baker, *Science*, 2019, **364**, 658–664.
26 E.-M. Strauch, S. J. Fleishman and D. Baker, *Proc. Natl. Acad. Sci. U. S. A.*, 2014, **111**, 675–680.
27 H. Watanabe, C. Yoshida, A. Ooishi, Y. Nakai, M. Ueda, Y. Isobe and S. Honda, *ACS Chem. Biol.*, 2019, **14**, 2729–2736.
28 T. Sulea, N. Rohani, J. Baardsnes, C. R. Corbeil, C. Deprez, Y. Cepero-Donates, A. Robert, J. D. Schrag, M. Parat, M. Duchesne, M. L. Jaramillo, E. O. Purisima and J. C. Zwaagstra, *mAbs*, 2020, **12**, 1682866.
29 M. Khanwalker, R. Fujita, J. Lee, E. Wilson, K. Ito, R. Asano, K. Ikebukuro, J. LaBelle and K. Sode, *Biosens. Bioelectron.*, 2022, **200**, 113901.
30 D. F. Lake, K. S. Lam, L. Peng and E. M. Hersh, *Mol. Immunol.*, 1994, **31**, 845–856.
31 J. Jumper, R. Evans, A. Pritzel, T. Green, M. Figurnov, O. Ronneberger, K. Tunyasuvunakool, R. Bates, A. Žídek, A. Potapenko, A. Bridgland, C. Meyer, S. A. A. Kohl, A. J. Ballard, A. Cowie, B. Romera-Paredes, S. Nikolov, R. Jain, J. Adler, T. Back, S. Petersen, D. Reiman, E. Clancy, M. Zielinski, M. Steinegger, M. Pacholska, T. Berghammer, S. Bodenstein, D. Silver, O. Vinyals, A. W. Senior, K. Kavukcuoglu, P. Kohli and D. Hassabis, *Nature*, 2021, **596**, 583–589.
32 D. Kozakov, D. R. Hall, B. Xia, K. A. Porter, D. Padhorny, C. Yueh, D. Beglov and S. Vajda, *Nat. Protoc.*, 2017, **12**, 255–278.
33 R. Brenke, D. R. Hall, G.-Y. Chuang, S. R. Comeau, T. Bohnuud, D. Beglov, O. Schueler-Furman, S. Vajda and D. Kozakov, *Bioinformatics*, 2012, **28**, 2608–2614.
34 J. Abramson, J. Adler, J. Dunger, R. Evans, T. Green, A. Pritzel, O. Ronneberger, L. Willmore, A. J. Ballard, J. Bambrick, S. W. Bodenstein, D. A. Evans, C.-C. Hung, M. O'Neill, D. Reiman, K. Tunyasuvunakool, Z. Wu, A. Žemgulytė, E. Arvaniti, C. Beattie, O. Bertolli, A. Bridgland, A. Cherepanov, M. Congreve, A. I. Cowen-Rivers, A. Cowie, M. Figurnov, F. B. Fuchs, H. Gladman, R. Jain, Y. A. Khan, C. M. R. Low, K. Perlin, A. Potapenko, P. Savy, S. Singh, A. Stecula, A. Thillaisundaram, C. Tong, S. Yakneen, E. D. Zhong, M. Zielinski, A. Žídek, V. Bapst, P. Kohli, M. Jaderberg, D. Hassabis and J. M. Jumper, *Nature*, 2024, **630**, 493–500.
35 J. P. V. Heuvel, in *Comprehensive Toxicology*, Elsevier, 2018, pp. 18–43.
36 P. D. Home, *Diabetes Obes. Metabol.*, 2012, **14**, 780–788.
37 J. P. Bantle, D. C. Laine, G. W. Castle, J. W. Thomas, B. J. Hoogwerf and F. C. Goetz, *N. Engl. J. Med.*, 1983, **309**, 7–12.
38 M. Poudineh, C. L. Maikawa, E. Y. Ma, J. Pan, D. Mamerow, Y. Hang, S. W. Baker, A. Beirami, A. Yoshikawa, M. Eisenstein, S. Kim, J. Vučković, E. A. Appel and H. T. Soh, *Nat. Biomed. Eng.*, 2020, **5**, 53–63.
39 C. Caucheteur, T. Guo and J. Albert, *Anal. Bioanal. Chem.*, 2015, **407**, 3883–3897.
40 P. Dauphin-Ducharme, K. Yang, N. Arroyo-Currás, K. L. Ploense, Y. Zhang, J. Gerson, M. Kurnik, T. E. Kippin, M. N. Stojanovic and K. W. Plaxco, *ACS Sens.*, 2019, **4**, 2832–2837.
41 V. Crivianu-Gaita and M. Thompson, *Biosens. Bioelectron.*, 2016, **85**, 32–45.
42 J. Coulm, D. Léonard, C. Desroches and F. Bessueille, *Colloids Surf., A*, 2015, **466**, 75–84.
43 D. B. Wolfe, J. C. Love, K. E. Paul, M. L. Chabinyc and G. M. Whitesides, *Appl. Phys. Lett.*, 2002, **80**, 2222–2224.
44 J. Y. Lichtenberg, Y. Ling and S. Kim, *Sensors*, 2019, **19**, 2488.
45 A. Frutiger, A. Tanno, S. Hwu, R. F. Tiefenauer, J. Vörös and N. Nakatsuka, *Chem. Rev.*, 2021, **121**, 8095–8160.
46 H. S. Magar, R. Y. A. Hassan and A. Mulchandani, *Sensors*, 2021, **21**, 6578.
47 S. A. Pullano, C. D. Critello, I. Mahbub, N. T. Tasneem, S. Shamsir, S. K. Islam, M. Greco and A. S. Fiorillo, *Sensors*, 2018, **18**, 4042.
48 R. M. Lubken, M. H. Bergkamp, A. M. De Jong and M. W. J. Prins, *ACS Sens.*, 2021, **6**, 4471–4481.
49 G. Rong, S. R. Corrie and H. A. Clark, *ACS Sens.*, 2017, **2**, 327–338.
50 A. D. Buskermolen, Y.-T. Lin, L. Van Smeden, R. B. Van Haaften, J. Yan, K. Sergelen, A. M. De Jong and M. W. J. Prins, *Nat. Commun.*, 2022, **13**, 6052.
51 G. Krainer, K. L. Saar, W. E. Arter, T. J. Welsh, M. A. Czekalska, R. P. B. Jacquat, Q. Peter, W. C. Traberg,

A. Pujari, A. K. Jayaram, P. Challa, C. G. Taylor, L.-M. Van Der Linden, T. Franzmann, R. M. Owens, S. Alberti, D. Klenerman and T. P. J. Knowles, *Nat. Commun.*, 2023, **14**, 653.

52 N. Maganzini, I. Thompson, B. Wilson and H. T. Soh, *Nat. Commun.*, 2022, **13**, 7072.

53 J. Das, S. Gomis, J. B. Chen, H. Yousefi, S. Ahmed, A. Mahmud, W. Zhou, E. H. Sargent and S. O. Kelley, *Nat. Chem.*, 2021, **13**, 428–434.

54 D. A. Gough, L. S. Kumosa, T. L. Routh, J. T. Lin and J. Y. Lucisano, *Sci. Transl. Med.*, 2010, **2**(42), 42ra53.

55 R. J. Soto, J. R. Hall, M. D. Brown, J. B. Taylor and M. H. Schoenfisch, *Anal. Chem.*, 2017, **89**, 276–299.

56 A. M. Downs and K. W. Plaxco, *ACS Sens.*, 2022, **7**, 2823–2832.

57 H. Zargartalebi, S. Mirzaie, A. GhavamiNejad, S. U. Ahmed, F. Esmaeili, A. Geraili, C. D. Flynn, D. Chang, J. Das, A. Abdrabou, E. H. Sargent and S. O. Kelley, *Science*, 2024, **386**, 1146–1153.